

The Influence of In-plane Anisotropy and Temperature on the Performance of AA2050-T84 Alloy

Nagaraj Ekabote

Assistant Professor
Department of Mechanical Engineering
KLE Technological University, Hubballi
India

AA2050-T84 alloy is a third-generation Al-Li alloy used in aircraft and space vehicles. The spars and ribs of aircraft wings and fuel tanks of space shuttle tanks must possess damage tolerance properties. In this work, the tensile and fracture test specimens were extracted from the principal directions of the 43 mm-thick AA2050-T84 alloy plate and experimentally investigated at -50°C , 24°C , and 150°C . The dependency of tensile and fracture toughness properties on in-plane anisotropy and test temperature was observed. Also, the in-plane anisotropy effect on crack initiation, propagation, and deviations from principal crack directions under Mode-I loading was discussed. The short transverse directional tensile and fracture toughness properties were lowest due to weakened grain boundaries originating from the T-84 state. Further, the effect of the in-plane anisotropy nature of the alloy on the extraction of aircraft wing components is discussed.

Keywords: AA2050-T84 alloy, in-plane anisotropy, Crack path deviation, ASTM E399, Damage tolerant property.

1. INTRODUCTION

Aircraft and space industries have been fascinated by Al-Li alloys for decades to achieve the desired specific stiffness, strength, and lower density. The inferiority concerning anisotropy and thermal instability of first- and second-generation Al-Li alloys resulted in modifications in the processing of next-generation Al-Li alloys. The history of usage and withdrawal of earlier generation Al-Li alloys from aircraft, helicopters, and space vehicles due to anisotropy, thermal instability, and strain rate dependency of mechanical properties are well documented [1-6]. First- and second-generation Al-Li alloys are susceptible to load rates, changes in mechanical properties caused by heat exposure, and the initiation of microcracks at cutouts and holes during secondary processes of component fabrication. The incompatibility of these Al-Li alloys in the service environments led to investigating the role and effect of the percentage of Lithium in Al-Li alloys. The distribution of precipitates and the size and density of grains are significantly influenced by the lithium-to-copper ratio (Li:Cu). Based on failure investigations, the restriction of Lithium addition ($< 2\%$) in the alloy with few controlled and innovative fabrication practices was proposed—also, the greater control over fabrication led to 3rd generation of Al-Li alloys with improved mechanical properties. The reduction in density of these alloys with an increase in Young's modulus and other mechanical properties resulted in enticing the primary components of aircraft and space application vehicles [2, 7, 8]. Presently, the advantages of these alloys have

led to their use in primary structures of modern transport aircraft and liquid propellant tanks of space vehicles.

The key properties useful in determining the suitability for critical parts of an aircraft are the alloy's strength, elastic modulus, and damage-tolerant properties (fatigue life, fatigue crack growth rate, and fracture toughness). Conventionally, the majority of experiments were conducted on standard specimens and later verified through actual component testing. Predictions of the damage-tolerant property of the alloy involve extensive and costly experiments. Hence, novel methods for evaluating the mechanical properties have been developed with the aim of reducing cost and time. The use of modern numerical methods and the extended finite element method (XFEM) has been reported to predict damage-tolerant properties [9-14]. The adoption of modern numerical methods in the aviation industry has greatly enhanced the efficiency and speed of designing and fabricating the critical components of aircraft.

AA2050-T84 is a 3rd generation Al-Li alloy used in the wing components (spars, ribs, and brackets) of Airbus A380 transport aircraft. The AA2050-T84 alloy can be made available in the form of plates of various thicknesses. This alloy benefits from a better combination of medium strength and toughness over the 2xxx and 7xxx series of aluminum alloys. The wing ribs of the A380 aircraft were fabricated using various thickened plates of AA2050-T84 alloy [15-19]. The advantage of improved resistance to stress corrosion over conventional aluminum alloys has led to the faster adaption of the new alloy. The tailor-made properties of the alloy and its improved resistance to stress corrosion when immersed in aircraft fuel require fewer inspections of the wing parts, thus reducing the cost of inspection [15].

Hafley et al. [20] reported the anisotropic behavior of the 100 mm thick AA2050-T84 alloy plate and

Received: October 2024, Accepted: April 2025

Correspondence to: Dr. Nagaraj Ekabote
Faculty of Mechanical Engineering, KLE Technological
University, Vidya Nagar, Hubballi, India

E-mail: ekaboenagaraj@gmail.com

doi: 10.5937/fme2502315E

© Faculty of Mechanical Engineering, Belgrade. All rights reserved

FME Transactions (2025) 53, 324-334 324

evaluated the alloy suitability to fuel tanks of the space launch vehicles. The investigation reported the superior mechanical properties over earlier used AA2195-made tanks at room and subzero (at -195°C) temperatures. However, most fracture toughness tests were unsuccessful because of crack path deviations from the principal direction. In contrast to the subzero temperatures, the anisotropic nature was more apparent at room temperature. Because of its nearly isotropic nature, the AA2050 alloy is a good choice for fuel tanks exposed to below-freezing temperatures [19, 20]. However, the brittle nature of the alloy at subzero temperatures with minimal percentage elongation is a cautious parameter. Likewise, Chemin et al. [21] noticed a decline in the fracture toughness of a 43 mm thick alloy from room temperature to subzero temperature (-54°C). In addition, the decreased temperature improved the tensile strength of the alloy, with unchanged ductility along the rolling direction. These direction-dependent properties of the alloy are crucial for extracting and fabricating the lower wing parts of the aircraft from the AA2050 plates.

Cracks in the wing brackets of Airbus A380 have been reported, which has led to a detailed inspection [22, 23]. Crack initiation in the lower wing parts was first reported in 2012. The inspection committee suggested adjusting the bracket fabrication sequence with holes and cutouts [24]. In addition, more frequent inspection intervals of existing Airbus wing structures are recommended for any possible crack growth. Recently, cracks near the spars and ribs of the wing were observed in Airbus A380 [22, 23]. These unpredicted cracks were related to exposure to different operating temperatures for an extended period during service [23]. A few Airbus A380 aircraft were scrapped with a service record of more than 15 years due to unanticipated cracks in rib feet originating at wing attachments and cracks in the outer rear end of the spar [23-24]. The thumb rule suggests using an alloy with a minimum elongation of 5% or more for the damage-tolerant property requirements of aircraft components [17]. However, Hafley et al. [20] reported a 4.5% and less elongation along the 45° to short transverse and rolling directions. Hence, the spar, rib, or bracket behavior depends on the extraction location and orientation of the alloy plate.

Earlier investigations [18, 25-28] of this alloy reported mechanical behavior dependency on temperature, specimen location and orientation extracted from the plate, plate thickness, and percentage of constituents present in the alloy. A less thick plate possesses greater yield and ultimate strength than large-thick plates. In addition, the percentage of elongation in less thick plates is greater in the respective orientations than in thick plates. The test temperatures considered in earlier studies were room and subzero temperatures. However, aircraft and space shuttles experience temperatures ranging from -50°C to 150°C during operation [17]. Hence, the suitability of a thinner AA2050-T84 plate for these applications in terms of key mechanical properties is essential.

The literature discussed, related to the suitability of AA2050-T84 alloy to aircraft wing critical parts and space applications, is inadequate to claim structural

integrity. Hence, this work aims to analyze the directional anisotropy and multiple crack initiation mechanisms of the AA2050-T84 alloy to upgrade the structural integrity assessments in the future. In addition, the present study aims to assist in the early detection of cracks in service by understanding the actual behavior of the alloy related to anisotropy, service loads, and crack path deviations. The integrated approach of directional anisotropy properties influences the crack path directions, and the formation of multiple cracks is helpful in representing realistic conditions during service.

In this work, the tensile and fracture test specimens were extracted from the principal directions of the 43 mm, AA2050-T84 alloy plate and experimentally investigated at -50° , 24° , and 150°C . The mechanical properties obtained from the tests were compared with respect to the test temperature and directional anisotropy.

Furthermore, issues related to in-plane anisotropy and crack path deviations from the principal crack directions under Mode-I loading were examined. Understanding the directional properties along with the initiation of multiple cracks helps extract and fabricate the critical components of the aircraft by choosing the proper orientation from the plate. Thus, linking micro-structural anisotropy with macro-scale crack behaviors helps to improve the existing numerical methods for evaluating the crack behavior and failure assessments of this alloy. Finally, the compatibility of the alloy for the aircraft wing parts with respect to structural integrity will be discussed.

2. MATERIAL AND EXPERIMENTAL TEST DETAILS

2.1 AA2050-T84 alloy

A 43 mm thick AA2050-T84 alloy plate was used for the extraction of the test specimens. The chemical compositions of the alloys are listed in Table 1. Due to the limitations of the Al-Li alloy from earlier generations, lithium was limited to 0.93%, which led to a decrease in density by 3% and an increase in the alloy's Young modulus by 6% [3, 15].

The chemical composition, as displayed in Table 1, is said to balance the strength and toughness, making it superior to other traditional aluminum alloys. Also, the Zinc (Zn) addition in the alloy improves the corrosion resistance properties suitable for application in aircraft wings. The alloy was rolled repeatedly during fabrication to attain the required plate thickness under a certain operating temperature. The fabrication of rolled plates ensures the required thickness with refined microstructure.

Table 1. Chemical composition of AA2050-T84 alloy (Wt%)

Si	Fe	Cu	Mn	Mg	Al
0.03	0.05	3.56	0.38	0.35	
Zn	Ti	Ag	Li	Zr	remaining
0.09	0.03	0.33	0.93	0.08	

2.2 Specimen Details

The principal directions considered in the study were the rolling (R), transverse (T), and thickness or short transverse (S) directions. The tensile and fracture

specimens extracted from different plate directions are shown in Figure 1. The tensile specimens were extracted in the RT (along rolling), TR (along transverse), and ST (along thickness) orientations. Similarly, the fracture toughness specimens were extracted along the R-T (load along the rolling direction and crack propagation along the transverse direction), T-R (load along the transverse direction and crack propagation along the rolling direction), and S-R (load along the short transverse direction and crack propagation along the rolling direction) directions. Three specimen samples were extracted along each considered direction for both tensile and fracture toughness. A total of 54 (27 tensile and 27 fracture toughness) specimens were extracted to cover all test temperatures and orientations.

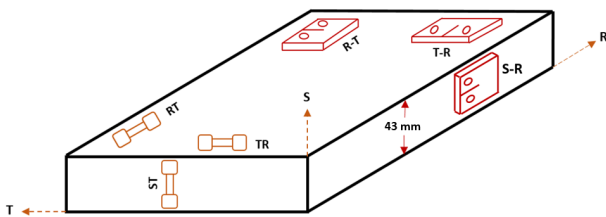


Figure 1. Various tensile and fracture toughness specimen orientations

Circular cross-sectioned tensile specimens with threaded ends were extracted according to ASTM E8, as shown in Figure 2 (a). A gauge diameter of 6 mm and a gauge length of 30 mm were used. The overall length of the specimens was 65 mm in both the RT and TR orientations. However, due to plate thickness restriction, the smaller tensile specimens were considered along ST orientations, as shown in Figure 2 (b).

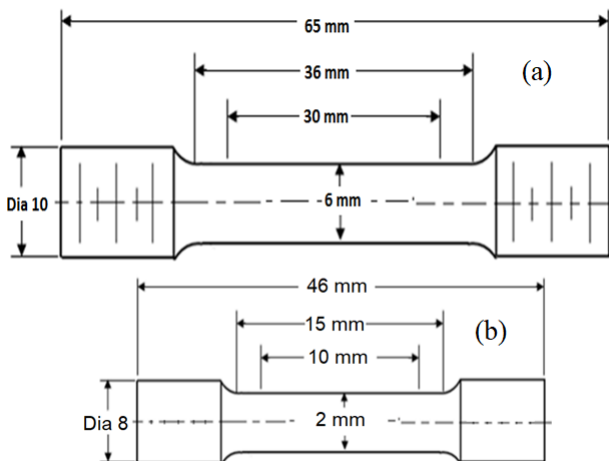


Figure 2. Tensile specimens for (a) RT and TR directions and (b) ST direction

Similarly, a Compact Tension (CT) specimen was used to conduct fracture toughness tests as per ASTM E399. The details of the CT specimen are shown in Figure 3. Both tensile and fracture toughness tests were conducted using a servo-hydraulic universal testing machine (UTM) of 100 kN capacity. Instruments such as load cells, extensometers (contact and non-contact type), and Crack Mouth Opening Displacement (COD) were also used to record the tensile and fracture toughness data. A noncontact-type extensometer was used during the high-temperature tests. Subzero and higher test temperatures were achieved using a furnace around

the test specimen mounted on the UTM. A typical experimental setup with fabricated tensile and fracture specimens is shown in Figure 4.

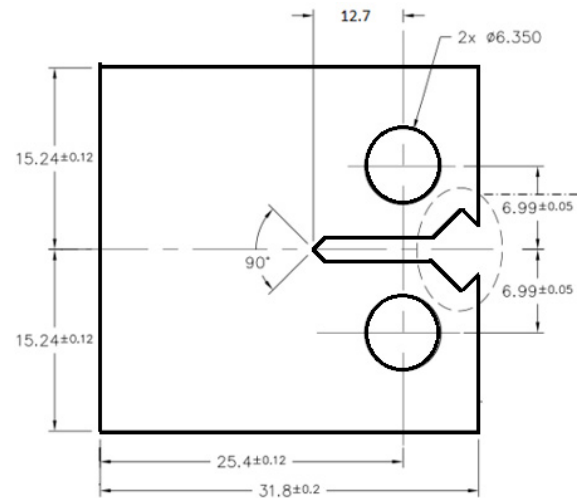


Figure 3. Compact Tension (CT) specimen

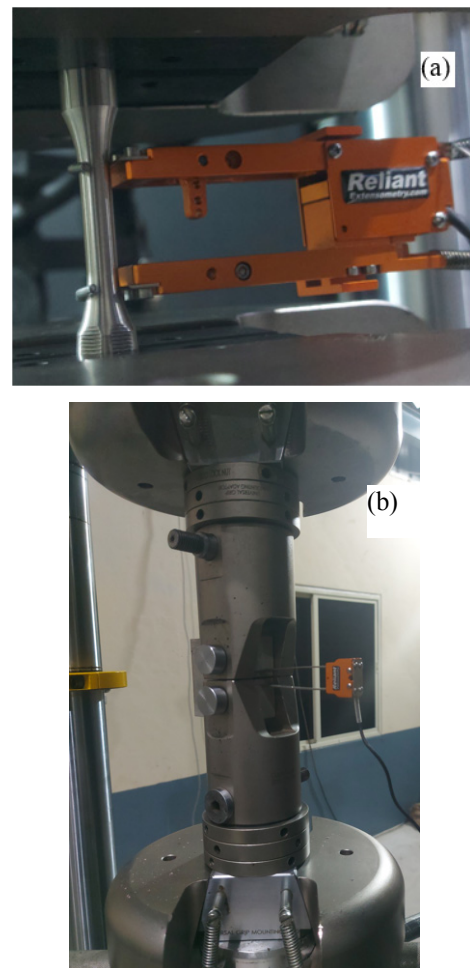


Figure 4. Experimental setup for (a) Tensile test (b) Fracture Toughness test

3. RESULTS AND DISCUSSIONS

Tensile and fracture toughness tests were conducted at various test temperatures and for orientation-specific specimens. The upcoming sections will discuss their effects on the key tensile and fracture toughness parameters.

3.1 Tensile test results and discussions

Tensile tests resulted in load versus deformation plots, which were further transformed into stress versus strain graphs. The vital tensile properties, such as yield stress (S_{yt}), ultimate stress (S_{ut}), Young's modulus (E), and % elongation, were extracted from the stress and strain graphs. Figure 5 shows the effect of test temperature and orientation on tensile properties.

In Figure 5 (a), a linear variation in yield stress with respect to specimen orientation was observed. Yield stress decreased in the RT, TR, and ST orientation sequences for all the test temperatures. Yield stress was highest at -50°C temperature and lowest at 150°C temperature for all the specimen orientations. The lowest magnitude of yield stress was noticed for ST orientation at 150°C temperature. Similarly, the highest magnitude of yield stress was witnessed for RT orientation at -50°C . The microstructural stability and effective precipitation strengthening led to the higher yield stress at -50°C for all specimen orientations [20, 21]. The slower diffusion rates and resistance to dislocation moments at -50°C enhanced the yield stress of the alloy. Also, the thermal activation energy at 150°C is higher, leading to an easier dislocation moment, and the alloy becomes softer, resulting in lesser yield stress than sub-zero temperature.

During the failure of the tensile specimen, the plastic strain (also, % elongation) was higher for RT and lower for ST. Higher plastic strain implies more load cycle withstanding capacity, which leads to higher yield stress. The rolling direction associated with elongated grains (RT direction) makes the stress flow paths smoother and thus enhances the load-carrying capacity. Meanwhile, the ST direction possesses the squeezed grains along the loading, resulting in increased stress concentrations between the grains. Therefore, the yield stress in ST orientation was lower compared to RT. Overall, the yield stress decreased in the order of RT-TR-ST orientations. Compared to yield stress, specimen orientations had a lesser effect on ultimate stress magnitudes. Ultimate stress magnitudes were highest at -50° degrees Celsius and lowest at 150° degrees Celsius, similar to yield stress. However, the TR and ST orientation tensile specimens produced the same magnitudes of ultimate stress across all test temperatures. A difference of around 5% was noticed between RT and ST orientation for all considered temperatures. Currently, the author is unable to quantify the explanation for specimen orientation's ineffectiveness on ultimate tensile stress and cannot locate relevant literature. However, a similar trend was reported by Hafley et al. [20] and Chemin et al. [21]. Overall, the sub-zero temperature exposure of critical components in aircraft and space launch vehicles prefers the AA 2050-T84 [20, 21].

The key tensile property in the damage tolerant part requirement is % elongation. The highest % elongation of 16% was witnessed along the rolling direction at 150°C temperature, indicating the alloy's ductility. Similarly, for -50°C and 24°C , along the rolling direction, the % elongation was around 10-12%. Along transverse orientation, the elongation was between 9.8 – 10.9%. Hence, the alloy's ductility is better along rolling and

transverse directions. However, the lowest % elongation of 5 - 6% was noticed along ST orientation for -50°C and 24°C .

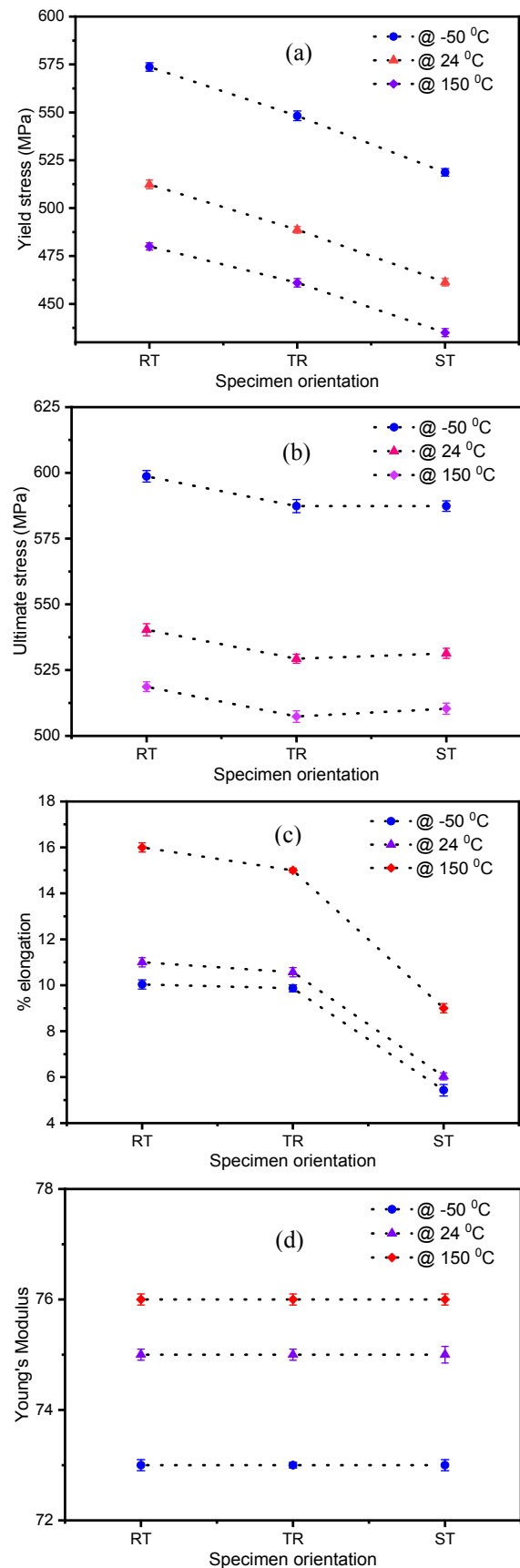


Figure 5. Temperature and orientation effect on (a) Yield stress (b) Ultimate stress (c) % elongation (d) Young's modulus

Meanwhile, the effect of specimen orientation on Young's modulus of the alloy is negligible, as seen in Figure 5 (d). The highest elasticity was witnessed at 150° C and the lowest at -50° C. The alloy exhibited the Young's modulus of 76 GPa at 150° C and 73 GPa at -50° C. Overall, as the temperature increases yield and ultimate stress decrease, and % elongation and Young's modulus of the alloy increases for all orientations. The rolling operation to obtain the required thickness of the plate induces the anisotropy related to orientation. Also, the penetration of the rolling-induced forces diminishes towards the plate center. However, the lesser thick plates exhibit effective transfer of rolling induced forces resulting in identical grain orientation both at the plate surface and center. The grain aspect ratio, which is the ratio of grain length to width is higher (an aspect ratio of almost 23 in the plate considered in this study) along the RT direction.

Typical broken tensile specimens at different test temperatures are shown in Figure 6. The ST orientation broken tensile specimens exhibited flat fractured surfaces, indicating the reduction in ductility of the alloy. However, rolling and transverse orientation broken tensile specimens displayed ductility-driven cup-cone fractured surfaces. The tensile specimen along the RT direction elongated more compared to the other two orientations for all considered temperatures. The plane of shear at 45° acting as the failure principal plane is the indication of ductility can be seen in Figure 6 for RT orientation. This behavior can be attributed to the elongated grains along the rolling direction associated with ductile nature. Similarly, along TR orientation the classical cup-cone fractured surfaces were visible representing ductile fracture. However, the elongation was a bit lower compared to RT-oriented tensile specimens.

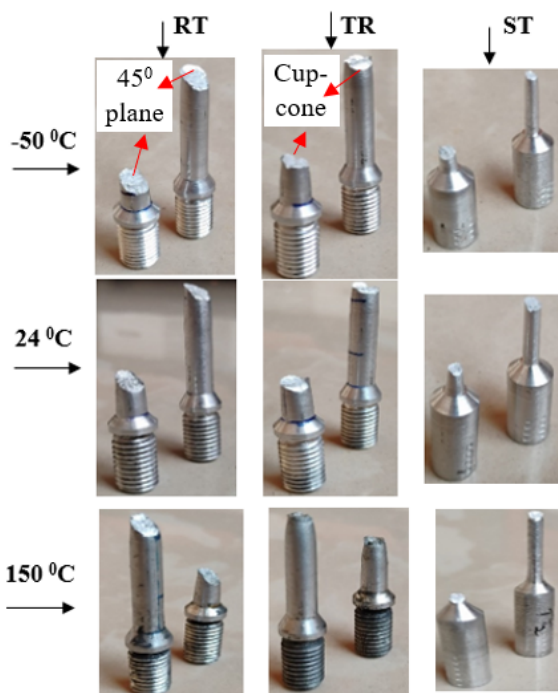


Figure 6. Broken specimens during tensile test

The aspect ratio of grain and size, play a major role in deciding the path of failure plane. Along ST

orientation, the miniature tensile specimens were used for testing and the broken specimens exhibited small dimpled flat surfaces. The reduction in % elongation of up to 50% compared to RT was noticed and brittle fractures were suspected. Hafley et al. [20] also reported a reduction in % elongation of about 45% between rolling and short transverse-orientated tensile specimens derived from a 100 mm thick AA2050-T84 alloy plate. The rolling operation resulted in elongated grains along the rolling direction and squeezed grain shapes in short transverse directions resulting the anisotropy. The anisotropy along in-plane and through-thickness were reported for AA2050-T84 alloy [20, 26, 29, 30]. Overall, the short transverse direction is susceptible to early fracture due to lower yield stress, ultimate stress, and % elongation compared to other orientation-derived tensile specimens.

3.2 Fracture toughness test results and discussions

The crack tip constraint of wing components resembles the higher constraint represented by the CT specimen [17, 20, 29]. Hence, the CT specimen with geometry as per the ASTM E399 is used in the present study. A notched specimen was fatigue-loaded to achieve the required crack length defined as a pre-cracking stage. The pre-cracking fatigue load is restricted in magnitude as defined by the ASTM E399 and depends on the fracture toughness of the alloy. Several thousands of fatigue cycles were applied to initiate the notched crack to a defined length (blue line in Figure 4). This pre-cracking will ensure the natural crack characteristics at the crack tip with high constraint. The pre-cracking step is essentially executed at room temperature and is a crucial step of valid fracture toughness test requirement. Further, the pre-cracked specimen was tested at required experimental conditions. Presently, R-T, T-R, and S-R orientation CT specimens were used at various test temperatures.

During fracture toughness testing, the Load-Line Displacements (LLD), applied load (P), and Crack Mouth Opening Displacements (COD) were recorded continuously. The load versus COD plot was further used to identify the critical load (P_Q) and led to the corresponding determination of the stress intensity factor (K_Q). The validity requirements of the standard tests were applied to check and declare the K_Q as the Plain Strain Fracture Toughness (K_{IC}) of the alloy. Figure 7 shows the magnitudes of K_{IC} for various orientations and test temperatures.

The alloy exhibited the lowest K_{IC} along S-R orientation for both sub-zero and room temperatures. Irrespective of the temperature, for all considered orientations the K_{IC} of the alloy decreased in the sequence of R-T, T-R, and S-R. At -50° C temperature, the K_{IC} of the alloy was lower by about 15% compared to room temperature. Similar observations of decreased K_{IC} of the alloy with a decrease in temperature were made by Chemin et al. [21]. The reduction of K_{IC} was associated with strain localizations and piling up of dislocations at the crack tip by increasing the constraint (stress concentration) at lower temperatures [21]. The S-R-oriented specimens showed almost non-dependency on

testing temperature. The major limitation of the second-generation Al-Li alloys was associated with lower toughness and has been attributed to higher Lithium presence in the alloy. Thus, the restriction of Lithium within 1% in AA2050-T84 alloy increased the fracture toughness by around 20% (along R-T orientation) compared to 2nd generation Al-Li alloys. The Lithium restriction ensured the improved resistance to brittle inter-granular fracture, confirmed also through the higher % elongation in tensile tests. The fractured surfaces both in tensile (Figure 6) and fracture toughness tests showed the crack initiation and propagation sites normally seen in ductile fractures.

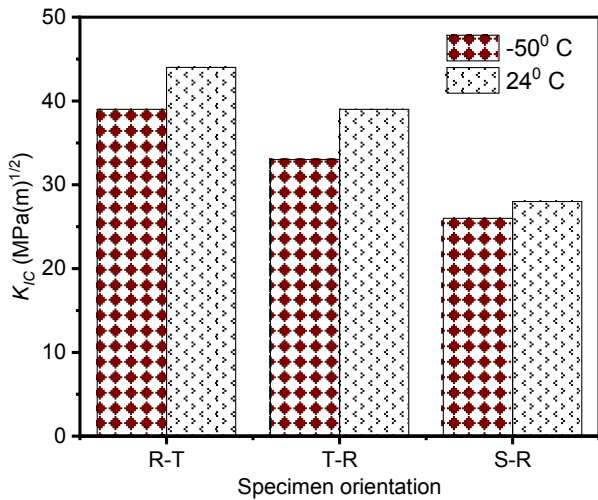


Figure 7. K_{IC} at various temperatures and orientations

The SEM images of fractured CT specimens are shown in Figure 8 for different temperatures. At room temperature, dimples of identical shape and size were created with few spots of inter-granular fractured surfaces indicating the ductility-driven crack propagation. The propagation path within grains is suggestive of plane stress conditions leading to higher toughness. Similarly, the concentration of dimples was minimal in fractured specimens of -50^o C. The increase in brittle inter-granular islands compared to room temperature SEM image can be visible. The constitute particles derived from Fe and Si alloying elements were present along the boundary of the grains. The segregation of alloying elements along the grain boundaries increases the strain localization and further triggers the areas of brittle intergranular fracture as observed. These microstructural features at -50^o C, accommodate the smaller plastic zones and lead to lower fracture energy [24-26] as witnessed in Figure 7.

At 150^o C, the alloy was more ductile compared to room temperature and showed crack blunting during the K_{IC} tests. The crack blunting resulted in a higher resistance to the crack propagation and eventually led to invalid K_{IC} tests.

However, the fracture toughness data reported by Ekabote et al. [28, 29] for 200^o C confirms the higher toughness of AA2050-T84 alloy compared to room, and sub-zero temperatures. Along with these successful fracture toughness tests, inconsistency in a few of the K_{IC} tests was also observed. The ample crack deviations

from the principal path of propagations were noticed during the K_{IC} tests.

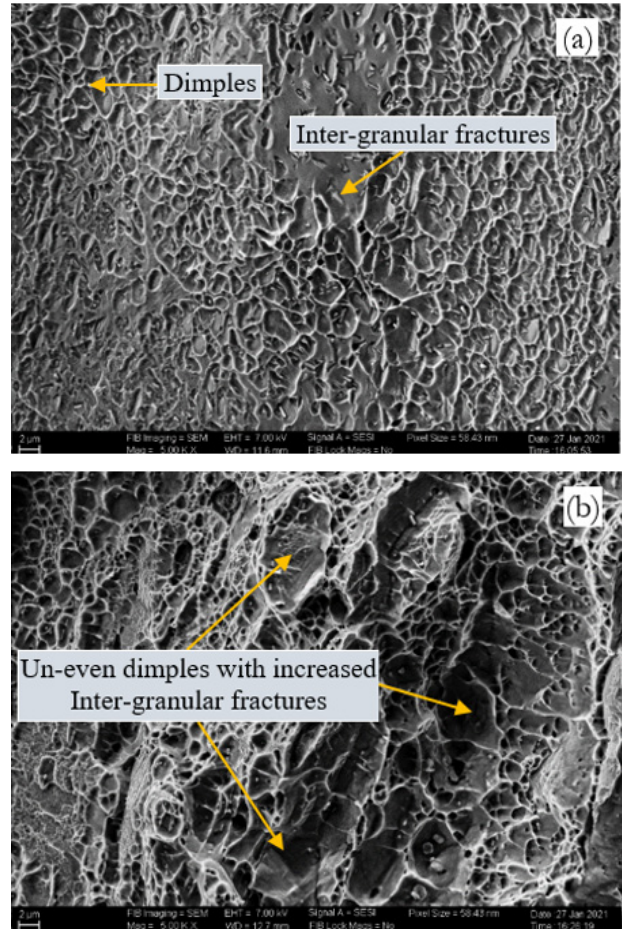
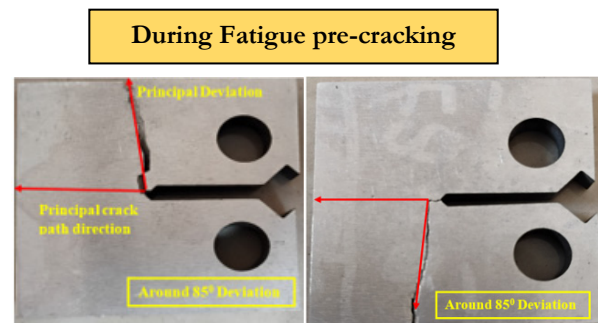


Figure 8. SEM images of fractured CT specimens at (a) 24^o C and (b) -50^o C

For all the test temperatures, the R-T orientation fracture specimens were shown path deviations for most of the samples. However, the control over wire cut minimum notch radius, fatigue loading frequency, and larger CT specimens (double the size mentioned in Figure 3) for R-T specimens ensured minimal crack deviations from the principal plane of propagation. The majority of CT specimen samples extracted through R-T for all considered temperatures showed crack path deviation from the principal propagation direction. The crack path deviations were observed in two instances. First, during the fatigue pre-cracking stage, and the second, while applying the tensile load for a fatigue pre-cracked CT specimen. The broken CT specimens with crack deviation are shown in Figure 9.



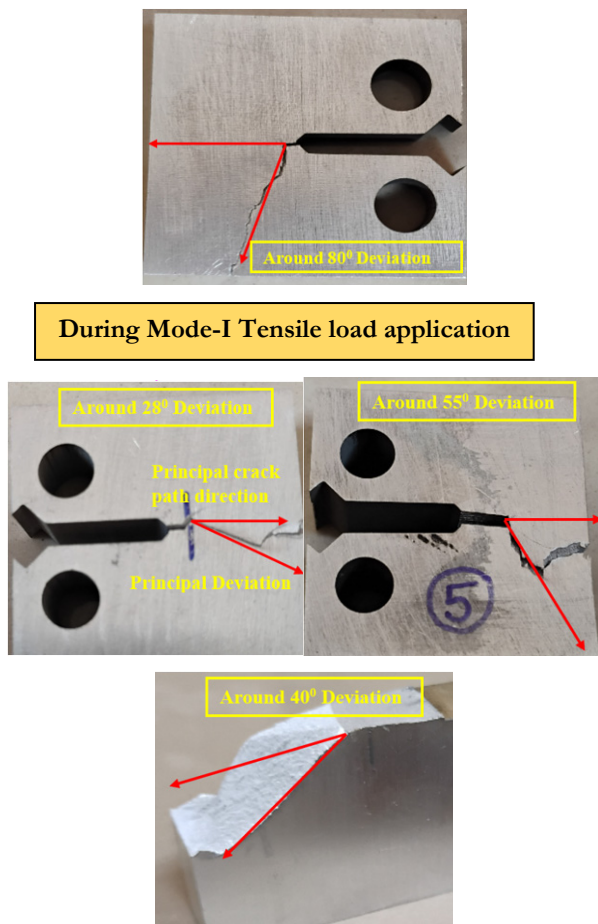


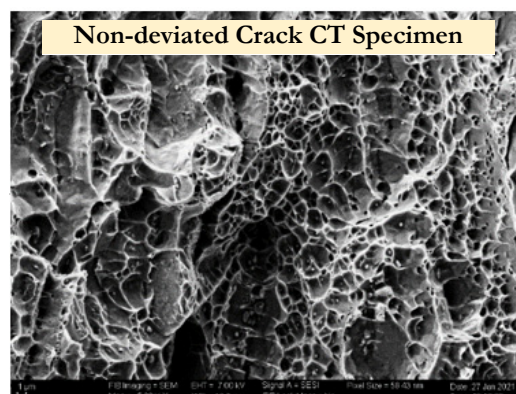
Figure 9. Broken CT specimens during K_{IC} tests

The fatigue pre-cracking stage displayed crack deviations of around 78° - 87° from the principal crack path for most of the R-T specimen samples. The crack path deviations were associated with grain structure and T-84 state-derived grain boundaries with misorientation angles [31]. During fatigue loading, the crack path chooses the misoriented grain boundary for the propagation. Similar kinds of crack path deviations were observed by Hafley et al. [20] for 100 mm thick AA2050-T84 alloy plate-derived CT specimens. The deviations were reported for thin CT specimens of thickness 6.35 mm during the J-resistance curve (involves loading and unloading cycles) determinations. Along with R-T orientation, the S-R-orientated CT specimens also show crack path deviations. In R-T oriented specimens, 40° - 45° angle of deviation, and for S-R oriented specimens, 45° - 60° angle of deviation were reported [20, 26, 30, 31]. Earlier literature on K_{IC} of the 2050-T84 alloy under Mode-I loading [28, 29] has not stated the crack path deviations. In the present work, the K_{IC} tests in R-T orientation produced both deviated and non-deviated crack paths. Few of the CT samples followed the principal crack path while propagating and obtaining a valid K_{IC} magnitude as per the standard mentioned in Figure 7. However, few have shown a deviation of 28° to 55° from the principal crack path while applying the Mode-I monotonic loading. These deviations are also along through-thickness direction S-R (short transverse direction) with uneven crack surfaces as shown in Figure 9. If the pre-cracking stage resulted in a crack tip with a micro deviation

angle, the Mode-I tensile load exhibited the deflection of crack paths as observed from crack tip root deflection.

The angle of deviation depends on the micro-structure and aspect ratio of the grain. The deviations of 40° - 60° were associated with grain aspect ratio. As the thickness of the plate increases, the rolling process causes less grain elongation and controllable aspect ratio resulting in minimal crack path deviations. In thick plates, the rolling process causes minimal grain elongations in the rolling direction ensuring a lower aspect ratio in R-T and S-R. In thin plates, the rolling process penetrates easily through the thickness of the plate producing the elongated grains and higher aspect ratio between R-T and S-R. During fatigue loading, these aspect ratios play a deciding role in choosing the crack propagation path as the slow and steady crack initiation and propagation occur. The AA2050-T84 alloy rolled plates are available from 25 mm to 152 mm thicknesses. It has been observed that in thick plates the grain aspect ratio at the center of the plate is lesser compared to the plate surface [21, 30]. Hence, fatigue loading results larger deviation angle in thin stock plate-derived CT specimens and a lesser deviation angle in thick stock plate-derived CT specimens. The presence of micro-cracks was noticed (especially towards the short transverse direction) in the fractured surfaces of Figure 9. The fractured specimens during pre-cracking fatigue loading stages may have micro-cracks at an angle of 70° - 90° from principal crack paths. The crystallographic structure of the alloy is the reason for crack deviation [4]. Figure 10 shows the micro-structural observations in CT specimens for valid and in-valid K_{IC} tests at room temperature.

The SEM images of deviated and non-deviated cracks at different microscales are shown in Figure 10. These microstructures can be differentiated by the type of fracture modes, inclusion intensity, and location, rolling effectiveness on grain, and formation of shear bands. Fracture modes include ductile or brittle fracture-driven intergranular or cleavage types. Inclusions are the other alloying elements influencing the crack initiation and sometimes deflection. Rolling operation in plate formation commonly affects the grain aspect ratio and orientation, resulting in the overall texture of the microstructure. Similarly, Shear bands are the indication of local plasticity during crack propagation. The micro-structure analysis of Figure 10 concerning these features is shown in Table 2.



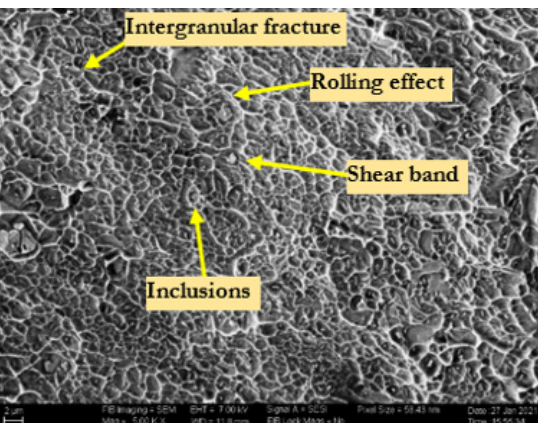
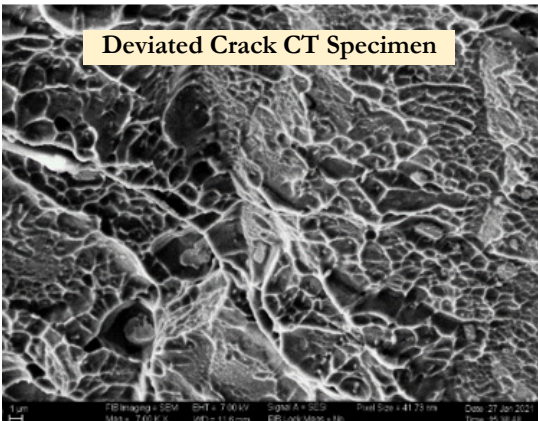
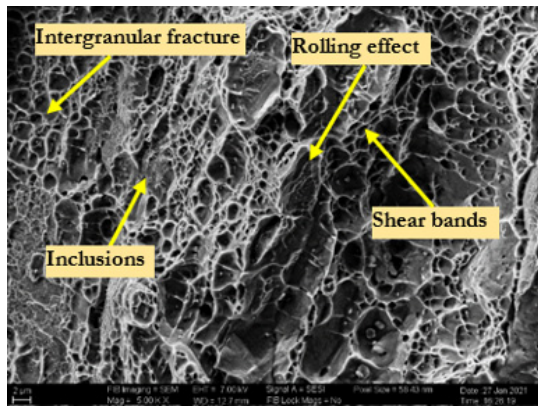


Figure 10. SEM images of CT fractured surfaces at room temperature

Table 2. Comparison of microstructural features in cracked CT specimens

Microstructural features	Non-deviated crack surface	Deviated crack surface
1. Fracture type	Irregular grain boundary fractures with secondary cracks.	Highly irregular and branched intergranular fractures.
2. Inclusions	Medium-sized inclusions causing crack initiation.	Dense inclusions with a mix of initiation and deflection.
3. Rolling effects	Noticeable grain elongation and texture change.	Extreme elongation and strong directional grain flow.
4. Shear bands	Shear bands were observed near large inclusions.	Widespread shear bands with severe localized plastic zones.

Thus, clear and differentiable microstructure changes in both types of crack propagation were witnessed through the above features. Both SEM images showed uneven grain boundaries, although more extensive branching was seen on deviated fracture surfaces. These branches resulted due to highly irregular grain boundaries. Similarly, secondary particles or inclusions in the matrix initiate the crack, but owing to segregation at one place has influenced the crack paths. The size of the inclusions was almost identical (for the majority portion) in both microstructure images, but deviations were produced from clusters of larger-sized secondary particles.

Rolling operation produces the elongated grains, and the aspect ratio of these grains is crucial to crack propagation directions. A detailed analysis of the aspect ratio on crack deflection is discussed in earlier literature [32]. The difference in elongation of the grains from the same plate can be attributed to CT specimen extraction from plate surfaces and below the surfaces. The plate surface exhibited larger elongated grains than sub-surface derived CT specimen grains. Shear bands are a clear indication of plasticity sites in the microstructure. The more populated shear bands were seen in deviated crack micro surfaces, leading to more considerable plasticity. Though the cracks deviated from the principal path, their toughness was slightly larger (almost 2%) than valid K_{IC} test results. Figure 11 helps to understand the intensity of these features' presence in both microstructures. The intensity was measured based on the presence of the features in the microstructure.

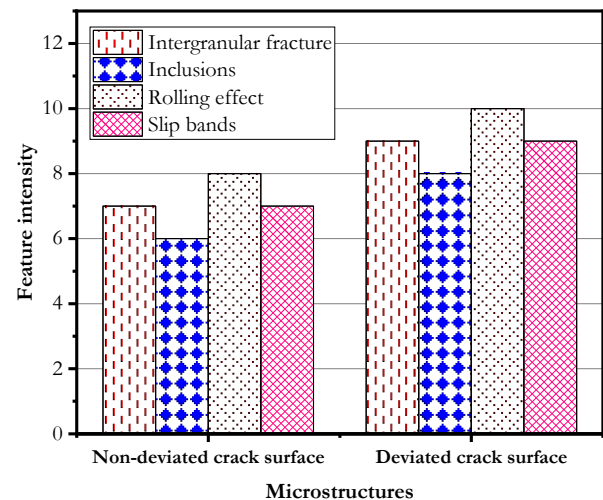


Figure 11. Comparison of feature impact across microstructures of deviated and non-deviated cracks

Figure 11 helps to clearly distinguish the impact of these features on crack path deviations seen in CT specimens. Each feature shows the 2-point extra intensity in deviated crack microstructure compared to non-deviated crack paths. The rolling process is the deciding feature as it affects the structure's inclusion distribution and slip band formation. If the rolling process is uniform and results in controllable grain sizes (aspect ratio), clustering of inclusions can be avoided, and fewer slip bands will be formed. Thus, it produces less irregular grain boundaries with intergranular fractures at room temperature. Also, in Figure 10, The microvoids or small dimples formation at room temperature represent the

local plastic deformation and resistance to the fracture phenomenon. The more significant number of micro voids in SEM images represents the more plasticity or ductility witnessed through the larger magnitude of K_{IC} and more % elongation during tensile tests. The dislocation movements were also more significant at room temperature. The anisotropy resulted in weaker grain boundaries along the S-R orientations and thus gave rise to crack initiation. The rolling operation on the plate squeezes the grains in the short transverse direction, and misoriented grains are formed. The fracture path was influenced by secondary particle segregation along the grain boundary at room and sub-zero temperatures. At room temperature, these particles help to distribute the stress, leading to plastic deformations. The difference in mechanical properties of secondary particles and alloy matrix leads to crack initiation at the interface. Sometimes, the piling up of secondary particles at large numbers along the grain boundary may deviate from the crack path and produce the intergranular fracture as witnessed in deviated crack path K_{IC} tests. The better processing of the alloy reduces the segregation of secondary particles and thus helps to propagate the crack in the principal path. The absence of crack deviations during K_{IC} tests at -50°C can be attributed to weakened grain boundary, less resistance for crack propagation, and reduction in ductility of the Aluminum matrix. Hence, the combined effect of anisotropy and temperature varied the nature of the alloy. The crack path deviations can be minimized by striking a balance between grain sizes, resulting in less anisotropy with an even distribution of the secondary particles.

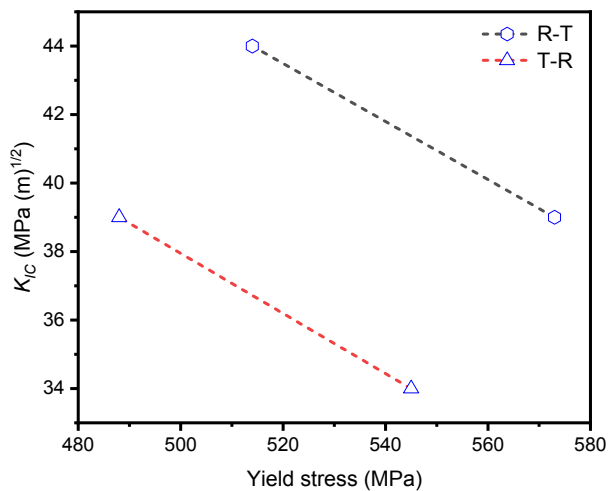


Figure 12. Relationship between yield stress and fracture toughness of the AA2050-T84 alloy

Further, the yield stress and fracture toughness obtained for different temperatures and orientations are used to derive the relationship between yield stress and fracture toughness. The relationship between fracture toughness and yield stress of the AA2050-T84 alloy is shown in Figure 12. The yield stress and fracture toughness were compared for R-T and T-R orientations. In conventional Aluminum alloys, yield stress and fracture toughness were inversely proportional. A similar behavior was witnessed for AA2050-T84 alloy for both the rolling and transverse directions. The secondary phases and precipitates improve the strength of the alloy

but act as stress concentration sites along the grain boundary. Hence, at low temperatures, the increase in strength also triggers the crack initiation from these sites, resulting in lower fracture toughness of the alloy. However, the conventional Aluminum alloys (AA7050) used in aircraft wing parts lack the right balance between yield stress and fracture toughness of the alloy compared to AA2050-T84. Thus, the use of AA2050-T84 alloys to damage tolerant property requirement parts of the aircraft justifies its selection. The additional advantage is the stress corrosion resistance property of the AA2050-T84 alloy due to other alloying elements mentioned in Table 1 necessary while immersed in the fuel of the aircraft wing.

The micro-crack's presence reveals the crack branching during fatigue loading of AA2050-T84 alloy. The presence of micro-cracks was minimal compared to 2nd generation Al-Li alloys [32]. The misorientation of grains at the crack tip is easy to propagate as witnessed in earlier literature [30, 31]. However, the fracture toughness of these deviated crack specimens was almost identical to the valid K_{IC} tests. Also, the tensile and fracture toughness properties of the AA2050-T84 alloy are higher than the earlier conventional Aluminum alloy (AA 7075), making it a better choice for aircraft wing parts applications. Meanwhile, these deviations will be difficult to inspect and to identify crack arrest directions in the wing parts. A more frequent inspection of AA2050-T84 alloy-made wing parts is necessary to achieve the structural integrity of the wing. Although novel experimental and numerical techniques for detecting component fractures have been published, they have not yet been included in aviation standards. [33-36]. Therefore, frequent inspection intervals increase the cost of maintenance but are essential to avoid sudden catastrophic failures.

Overall, the present investigation revealed the anisotropy-related tensile and fracture toughness properties of the 43 mm thick AA2050-T84 alloy. The guideline for selecting primary aircraft structures with damage-tolerant properties requirement necessitates a minimum elongation of 5% as one of the criteria [17]. Thus, the short transverse orientation lacks the ductility or minimum elongation (or is almost on the verge of) needed for wing spars and ribs. The Type-I and Type-II cracks in Airbus A380 may be related to minimum fracture toughness along the S-R orientation at lower temperatures. The short transverse orientation also has the lowest % elongation before fracture as reported through tensile tests. Together, temperature and in-plane anisotropy may have led to the crack appearances in wing brackets. Further, the wing components demonstrate elevated stress concentration points due to holes and cut-outs. These stress concentration points in the parts diminish the strength and toughness leading to crack initiation and propagation as visualized in the wing brackets. However, the higher constraint CT specimen represents these stress-concentrated effects in the Mode-I fracture toughness testing. Hence, the spars, ribs, and brackets of aircraft wings must be extracted along the rolling or transverse directions of the plate stock to satisfy the minimum damage-tolerant property requirement. This will ensure moderate ductility and tough-

ness coupled with elevated yield and ultimate strength in the loading axes, guaranteeing the structural integrity of the aircraft.

4. CONCLUSIONS

The rising concerns over the crack appearances in wing parts of the Airbus A380 triggered the inspection of essential mechanical and fracture toughness property evaluation of AA2050-T84 alloy and anisotropic nature dependency. The experimental investigation of the 43 mm plate-derived tensile and CT specimens showed improved characteristics over the conventional AA7050 alloy. Operating temperature, anisotropy, and plate thickness are key factors in selecting and extracting the wing parts from alloy plates. The major findings of the present work are concluded below.

- In tensile testing, an increase in testing temperature decreased the yield and ultimate stress of the alloy. In-plane anisotropy was witnessed, and the yield and ultimate stresses were decreased in the RT, TR, and ST orientation sequence for all considered temperatures. The short transverse direction possesses a lower % elongation with a brittle nature at subzero temperature, making the ST direction-derived parts non-suitable to wing primary components.
- During fracture toughness tests, a decrease in test temperature induced the brittle nature of alloy with lower K_{IC} . The clear patches of intergranular sites were visible in SEM images resulting in lower fracture energy. However, the alloy's ductility increased at higher temperatures, and the elastic-plastic fracture toughness (J -integral) parameter was suggested for toughness evaluation owing to crack blunting.
- Crack path deflections were observed in R-T and S-R orientation-derived CT specimens. Path deflection can be attributed to weakened grain boundaries in the T-84 state, misorientation angles of grains in transverse directions, and a higher aspect ratio of the grains. However, these orientation-specific fracture toughness magnitudes are more significant than the earlier AA7050 alloy at subzero temperatures, making AA2050-T84 alloy a superior choice for aircraft wing parts.
- The wing's primary components must be extracted along the R-T or T-R orientations for better structural integrity of the aircraft wing. Avoiding the short transverse direction loading and crack propagation ensures the required damage-tolerant property for wing parts.

ACKNOWLEDGMENT

The author thanks the KLE Technological University for the financial support under the capacity building fund.

REFERENCES

- [1] Prasad, N. Eswara, Amol Gokhale, and Russell JH Wanhill, eds.: *Aluminum-lithium alloys: processing, properties, and applications*. Butterworth-Heinemann, 2013.
- [2] Abd El-Aty A, Xu Y, Guo X, Zhang SH, Ma Y, Chen D.: Strengthening mechanisms, deformation behavior, and anisotropic mechanical properties of Al-Li alloys, A review. *Journal of Advanced Research*, 10:49-67, 2018.
- [3] Starke EA, Sanders TH, Palmer IG.: New approaches to alloy development in the Al-Li system. *JOM*, 33:24-33, 1981.
- [4] Rioja RJ, Liu J.: The evolution of Al-Li base products for aerospace and space applications. *Metallurgical and Materials Transactions A.*, 43(9):3325-37, 2012.
- [5] Zou, C.L., Geng, G.H. and Chen, W.Y.: Development and application of aluminium-lithium alloy. *Applied Mechanics and Materials*, 599, pp.12-17, 2014.
- [6] Xiao, G., An, R., Yang, J. and Ma, J.: Research Progress of New Generation of Aluminum-Lithium Alloys Alloying. *Advanced Engineering Materials*, 26(12), p.2301639, 2024.
- [7] Kaya, E., Sheikhi, M.R., Gürgen, S., Kuşhan, M.C.: Aluminum-Lithium Alloys in Aircraft Structures. In: Kuşhan, M.C., Gürgen, S., Sofuoğlu, M.A. (eds) *Materials, Structures and Manufacturing for Aircraft. Sustainable Aviation*. Springer, Cham. pp. 1–25, 2022.
- [8] Alam, M.P. and Sinha, A.N.: Fabrication of third generation Al-Li alloy by friction stir welding: a review. *Sādhanā*, 44(6), p.153, 2019.
- [9] Grbovic, A., Rasuo, B.: FEM based fatigue crack growth predictions for spar of light aircraft under variable amplitude loading. *Engineering Failure Analysis*, 26, pp.50-64. 2012.
- [10] Grbović, A., Rašuo, B.: Use of modern numerical methods for fatigue life predictions. *Recent Trends in Fatigue Design*, pp.31-73. 2014.
- [11] Petrašinović, D., Rašuo, B., Petrašinović, N.: Extended finite element method (XFEM) applied to aircraft duralumin spar fatigue life estimation. *Tehnički vjesnik*, 19(3), pp.557-562, 2012.
- [12] Petrašinović, N., Petrašinović, D., Rašuo, B., Milković, D.: Aircraft duraluminum wing spar fatigue testing. *FME Transactions*, 45(4), pp.531-536, 2017.
- [13] Kastratović, G., Vidanović, N., Grbović, A., Rašuo, B.: Approximate determination of stress intensity factor for the case of multiple surface cracks. *FME Transactions*, 46 (1), pp.39-45, 2018.
- [14] Farah, S., Khalfallah, S., Boutemedjet, A., Rebhi, L.: A Design Optimization Strategy of an Aircraft Composite Wing-Box Based on a Multi-scale FEA. *FME Transactions*, 53(1), pp.157-172, 2025.
- [15] Rasposienko, D. Y. et al.: Multicomponent Aging Al-Li-Based Alloys of the Latest Generation: Structural and Phase Transformations, Treatments, Properties, and Future Prospects. *Materials*, 15(12), 4190, 2022.
- [16] Lequeu, P., Smith, K. P., & Daniélou, A.: Aluminum-copper-lithium alloy 2050 developed for med-

- ium to thick plate. *Journal of Materials Engineering and Performance*, 19, pp. 841-847, 2010.
- [17] Wanhill, R. J. H., Bray, G. H.: Aerostructural design and its application to aluminum–lithium alloys. In *Aluminum-lithium alloys*, Butterworth-Heinemann, 2014.
- [18] Ekabote, N., Kodancha, K.G., Khan, T.Y., Badruddin, I.A.: Effect of strain rate and temperature on tensile and fracture performance of AA2050-T84 alloy. *Materials*, 15(4), p.1590, 2022.
- [19] Zhu, L., Li, N., & Childs, P. R. N.: Light-weighting in aerospace component and system design. *Propulsion and Power Research*, 7(2), 103-119, 2018.
- [20] Hafley, R. A., Domack, M. S., Hales, S. J., & Shenoy, R. N.: Evaluation of Aluminum Alloy 2050-T84 Microstructure and Mechanical Properties at Ambient and Cryogenic Temperatures, NASA Langley Research Center. Report number: NASA/TM-2011-217163, 2011.
- [21] Chemin, A. E. A., Afonso, C. M., Pascoal, F. A., Maciel, C. I. D. S., Ruchert, C. O. F. T., & Bose Filho, W. W.: Characterization of phases, tensile aluminum alloys, *Material Design & Processing Communications*, 1(4), pp.1-13, 2019.
- [22] Jens Flottau.: Airbus identifies heat, humidity As causes Of A380 wing-spar cracking. Available at: Airbus Identifies Heat, Humidity as Causes of A380 Wing-Spar Cracking, Aviation Week Network, 2023.
- [23] Rytis Beresnevičius.: EASA targets oldest Airbus A380s for wing crack inspections. Available at: EASA Targets Oldest Airbus A380s For Wing Crack Inspections, 2024.
- [24] Reuters: More cracks found in Airbus A380 wings. Available at: More cracks found in Airbus A380 wings | Reuters, 2012.
- [25] Ekabote, N., & Kodancha, K. G.: Temperature and test specimen thickness (TST) effect on tensile and fracture behavior of AA2050-T84 alloy. *Materials Today: Proceedings*, 59, 673-678, 2022.
- [26] Tufan, B. A. et al.: Microstructural Anisotropy, Mechanical Properties, and Fatigue Crack Growth Behavior of AA2050-T84 Alloy. *Fatigue & Fracture of Engineering Materials & Structures*, 2024.
- [27] Kodancha, K., Ekabote, N., & Revankar, P. P.: Elastic-plastic fracture analysis of anisotropy effect on AA2050-T84 alloy at different temperatures: A numerical study. *Frattura ed Integrità Strutturale*, 16(59), 78-88, 2022.
- [28] Ekabote, N., & Kodancha, K. G.: Effect of loading rate on tensile and fracture behavior of AA2050-T84 alloy at high temperature. In *Journal of Physics: Conference Series*, Vol. 2070, No. 1, p. 012163, IOP Publishing, 2021.
- [29] Ekabote, N.: *Constraint Issues in Fracture Toughness of AA2050 T84 Alloy*. Ph.D thesis, KLE Technological University, Hubballi. Available at: <http://hdl.handle.net/10603/497806>, 2022.
- [30] Ata Tufan, B.: *Fatigue crack growth behavior of hot rolled aa2050-t84 plates*, Master of Science thesis, Middle East Technical University. Available at: <https://open.metu.edu.tr/handle/11511/105408>, 2023.
- [31] Esin, V. A., François, M., Belkacemi, L. T., Irmer, D., Briez, L., Proudhon, H.: Effect of microstructure on fatigue crack deviation in AA2050-T84, *Materials Science and Engineering: A*, 858, 144120, 2022.
- [32] Lynch, S. P., Wanhill, R. J. H., Byrnes, R. T., Bray, G. H.: Fracture toughness and fracture modes of aerospace aluminum–lithium alloys. In *Aluminum-lithium alloys*, pp. 415-455. Butterworth-Heinemann, 2014.
- [33] Shakir, S.M. and Jaber, A.A: Innovative Application of Artificial Neural Networks for Effective Rotational Shaft Crack Localization. *FME Transactions*, 52(1), 2024.
- [34] Federovich, S., Anatolyevich, K., Alexandrovich, C., Alexandrovich, E., Tanović, D. and Petrovich, M.: Application of chemography method to study surface damage phenomena. *FME Transactions*, 50, pp.484-490, 2022.
- [35] Jovičić, G., Živković, M. and Jovičić, N.: Numerical modeling of crack growth using the level set fast marching method. *FME Transactions*, 33(1), pp.11-19, 2005.
- [36] Ekabote N.: Investigating the constraint role in J-CTOD relationship for compact tension (CT) specimen. *Res. Eng. Struct. Mater.*; 11(2): 481-494, 2025. DOI: 10.17515/resm2024.251me0419rs.

УТИЦАЈ АНИЗОТРОПИЈЕ У РАВНИ И ТЕМПЕРАТУРЕ НА ПЕРФОРМАНСЕ ЛЕГУРЕ AA2050-T84

Н. Екаботе

Легура AA2050-T84 је Al-Li легура треће генерације која се користи у авионима и свемирским возилима. Носачи и ребра крила авиона и резервоари за гориво свемирских шатлова морају поседовати својства толеранције на оштећења. У овом раду, узорци за испитивање затезања и лома су извађени из главних праваца плоче легуре AA2050-T84 дебљине 43 mm и експериментално испитани на -500°C, 240°C и 1500°C. Посматрана је зависност својстава затезне и жилавости лома од анизотропије у равни и температуре испитивања. Такође, разматран је ефекат анизотропије у равни на настанак, ширење и одступања од главних праваца пукотина под оптерећењем у режиму I. Својства краткотрајне попречне затезне и жилавости лома била су најнижа због ослабљених граница зрна које потичу из стања T-84. Даље, разматран је ефекат природе анизотропије у равни легуре на извлачење компоненти крила авиона.